Photolithography at 193 nm

M. Rothschild, R. B. Goodman, M. A. Hartney, et al.

Citation: Journal of Vacuum Science & Technology B: Microelectronics and Nanometer Structures Processing, Measurement, and Phenomena **10**, 2989 (1992); doi: 10.1116/1.585958

View online: https://doi.org/10.1116/1.585958

View Table of Contents: https://avs.scitation.org/toc/jvn/10/6

Published by the American Institute of Physics

Photolithography at 193 nm

M. Rothschild, R. B. Goodman, M. A. Hartney, M. W. Horn, R. R. Kunz,
J. H. C. Sedlacek, and D. C. Shaver
Lincoln Laboratory, Massachusetts Institute of Technology, Lexington, Massachusetts 02173

(Received 24 July 1992; accepted 12 August 1992)

Photolithography at 193 nm is a natural continuation of the progression from 436 to 365 to 248 nm in lithography, dictated by the requirement for continually higher resolution. It is anticipated that 193-nm lithography will enable 0.25-μm patterning in volume production with conventional masks, and 0.18-μm resolution with phase-shifting masks. The main issues related to lithography at this new wavelength are being addressed. It has been shown that highly transparent optical materials are available at 193 nm. Also, they are damaged by the laser radiation at a slow enough rate that high-quality projection optics are expected to perform within specifications for ten years of full-time operation. Consequently, a 193-nm step-and-scan system is being constructed, and it has been designed to attain 0.25-μm resolution over a 22 by 35 mm field. A range of 193-nm photoresist schemes has been demonstrated. They include semitransparent single-layer resists, positive-tone surface imaging (silylation), and negative-tone bilayers using ultrathin silicon-based polymers. In most instances we have demonstrated sub-0.25-μm resolution, high photosensitivity, good exposure–defocus latitude, and very low levels of etch residue. In sum, the first successful steps towards a fully engineered 193-nm photolithography have been taken, and no major obstacles are anticipated.

I. INTRODUCTION

Photolithography has historically been the mainstream technology for volume production of integrated circuits (ICs). As successive generations of ICs required smaller and smaller features, the lithographic process based on *g*-line (436 nm) steppers was continually improved to obtain the required resolution. By the mid-1980's, micrometer and even submicrometer patterning was achieved, mainly due to increased numerical apertures (NA) of the projection optics and improved photoresist technologies. In terms of the lithographic equation $L=k_1\lambda/\mathrm{NA}$ (where L is the linewidth, k_1 is a process-dependent parameter, λ is the wavelength, and NA is the numerical aperture), the improvements in resolution up to that point were achieved by lowering k_1 or increasing NA. However, as the critical dimension of ICs approached 0.5-μm, it became apparent that λ had to be reduced as well. Indeed, *i*-line (365 nm) steppers are currently being used for 4 and 16 Mbyte dynamic random access memory (DRAM) production. Projecting into the future, it appears that improved illumination schemes and phase-shifting mask technologies may extend the resolution obtainable with *i*-line to $\sim$0.35 μm, albeit at the cost of added process complexity. The 0.25–0.35 μm domain will be reached mainly with 248–250 nm steppers (or step-and-scan systems), and the sub-0.25-μm regime is expected to employ 193-nm optics. At 193 nm 0.25-μm devices can be fabricated with conventional masks using projection optics with a relatively conservative NA of 0.5. Phase-shifting mask techniques similar to those currently being developed at longer wavelengths will then enable printing with 0.18-μm resolution, and in special geometries, down to 0.10 μm.

At Lincoln Laboratory we have been conducting a program to extend optical lithography to 0.25-μm resolution using a 193-nm, ArF excimer laser. We have pursued in parallel the development of the two main elements in a lithographic system: a stepper and resist processes. In both areas there has been significant progress, and 0.25-μm lithography at 193 nm appears now to be a viable technology. In this article we describe some of the key results of our work in this area.

II. PROJECTION OPTICS

A. System

A 193-nm step-and-scan system is presently being constructed by SVG Lithography under a subcontract to Lincoln Laboratory. It employs an optical design similar to that of the Micrascan 92: 4$\times$ reduction optics with 0.5 NA, and a full scanned field of 22 by 35 mm. The optical design can accommodate a relatively large bandwidth, and therefore no narrowing of the laser linewidth is required.

B. Optical materials

Many of the optical elements in the system being built by SVG Lithography are of the refractive type. Accordingly, one of the main areas of concern has been the availability and performance of transmissive optical materials at 193 nm. Because of the high photon energy, $\sim$6.4 eV, few optical materials are available with appropriately large band gaps. The class of transparent materials at 193 nm includes high-purity fused silica and several crystalline fluorides (CaF_2, MgF_2, LiF, NaF). Fused silica has been by far the preferred choice for 193-nm applications for a number of practical reasons: it is environmentally stable (the fluorides are hygroscopic to various degrees), and it can be polished to a very high degree of surface flatness. We have studied all of the materials listed above, with special emphasis on fused silica. The wavelength-dependent properties that have been addressed are the absorption coefficient and material stability under prolonged 193-nm irradiation.

 0734-211X/92/062989-08$01.00

1. Fused silica

Ultraviolet (UV)-grade fused silica can be obtained commercially from several primary sources. While the fabrication processes may differ, all high-quality grades have metallic impurities at or below the parts per million level. They are frequently classified by their content of hydroxyl groups as "wet" or "dry." We determined early on that dry fused silica (OH concentration below ~10 ppm) degrades much more rapidly when irradiated with 193-nm lasers than its wet (~300–1200 ppm OH) counterpart. Consequently, our studies have focused primarily on the latter type.

The absorption coefficient at 193 nm of wet fused silica can cover a wide range, even when provided by the same supplier and manufactured under nominally identical conditions. The vendors have been steadily improving their quality control and their understanding of the effects of certain process variations. The absorption coefficient is frequently in the range of 0.02–0.07 cm^{-1} (base *e*, assuming Beer's law). However, the intrinsic absorption of fused silica is probably much better. In fact, we have measured values of 0.007 cm^{-1}, even in large (10–15 cm thick) pieces. In these samples we could determine that the central part (~5–10 cm) has an even lower absorption coefficient, ~0.005 cm^{-1}. It is apparent from these results that highly transparent fused silica is indeed obtainable for 193-nm applications; the frequently observed higher losses may be attributed to residual impurities or to intrinsic defects, whose densities can be significantly reduced.

The presence, nature, and extent of gradual laser-induced changes in fused silica have been the subject of detailed studies by us. Briefly, two radiation-induced effects are observed.[1] One is formation of point defects, denoted E' centers, which are essentially charged oxygen vacancies. The E' centers manifest themselves as absorption features centered at ~215 nm, with sufficient width to contribute to absorption at 193 nm. Therefore, irradiation at 193 nm will cause increased absorption at this wavelength. The added absorption in turn has two major implications with respect to the performance of a high-quality optical system: (i) the overall transmission is degraded over time, and (ii) the absorbed fraction of 193-nm light causes local heating, which changes the refractive index of fused silica. In fact, the index of fused silica is quite sensitive to temperature changes, and at 193-nm it increases by $\sim 2\times10^{-5}$/°C of temperature rise. In order to keep index inhomogeneities to the desired ppm level, it is thus necessary that the laser-induced heating effects be kept to within a fraction of a degree.

The second laser-induced change in fused silica is a macroscopic densification (compaction) of the material. This effect can be directly observed with phase-measuring interferometers, or indirectly via the stress-induced birefringence near the perimeter of the irradiated area, where the fused silica is in a transitional stage between the compacted and uncompacted zones. The compaction causes a reduction in the geometrical pathlength and concurrently an increase in index of refraction. The net effect is a decrease in optical pathlength.

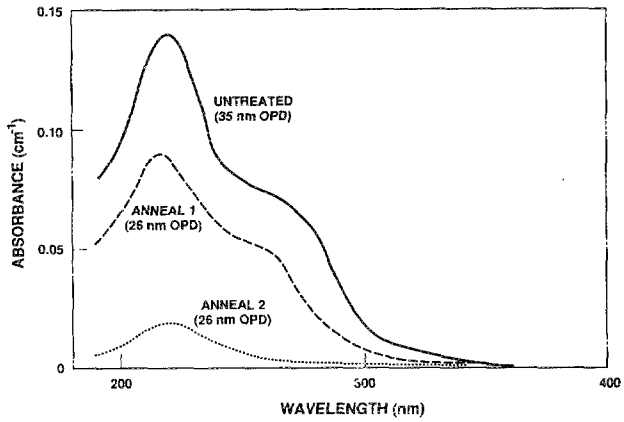

FIG. 1. Effect of annealing conditions during manufacturing of fused silica on 193-nm-induced color center formation. The absorption curves for three samples are shown, each sample having been exposed to 2×10^6 pulses at 78 mJ cm^{-2}/pulse. The absorption curves are normalized with respect to unirradiated portions of the respective samples, in order to eliminate differences in initial absorption. The values of laser-induced compaction are indicated in parentheses as optical path differences (OPD) between exposed and unexposed portions of the respective samples.

For a given sample, both the concentration of E' centers and the degree of compaction increase quadratically with laser fluence and linearly with the number of pulses, as would be expected from a two-photon induced process. Saturation is observed only at relatively high fluences (over ~70 mJ cm^{-2}/pulse), after $\sim 2\times10^6$ pulses.

It is important to note that, while the effects described above are observed in all the types of fused silica studied by us, their magnitude varies significantly with supplier, grade, and other more subtle manufacturing process conditions. Indeed, appropriately designed preirradiation processing was shown to reduce the 193-nm-induced absorbance by more than an order of magnitude for certain grades of fused silica (Fig. 1). The degree of irradiation-induced compaction appears to be much less affected by the same treatment.

For the purpose of predicting the useful lifetime of optical elements in a 193-nm projection system, we have used a simple numerical model. The most damage-prone element is the lens closest to the wafer, where the spot size is smallest and the fluence is highest. For this element we chose the best fused silica, in which the laser-induced changes in absorption are negligible, assumed a conservatively high fluence of 0.5 mJ cm^{-2}/pulse, and a maximum allowable compaction-induced optical path change of 1 ppm. It should be noted that the other optical elements will experience significantly less compaction, because of the reduced fluence. For a photoresist sensitivity of 10 mJ cm^{-2} the value of 1 ppm is reached, according to our calculations, in approximately ten years of full-time operation in a production-type environment. This result is extremely significant. It predicts that, because of the quadratic dependence on fluence and the 0.5 mJ cm^{-2}/pulse mentioned above, the laser-induced effects that are so readily observed in the laboratory at 10–100 mJ cm^{-2}/pulse have negligible

impact on the useful lifetime of a 193-nm step-and-scan system, provided carefully preselected fused silica is being used.

2. Fluorides

The most promising fluoride for use as an optical material at 193 nm is CaF_2. It is not as hygroscopic as LiF, it is not birefringent like MgF_2, it is mechanically less brittle than NaF or BaF_2, and it can be grown in relatively large crystals (6–8 in. in diameter).

In our studies all the fluorides developed laser-induced color centers, but no compaction of the type seen in fused silica has been observed. At the fluences used in our studies, ~ 100 mJ cm^{-2}/pulse, these centers are frequently formed within the first few hundred thousand pulses, and their concentration (as determined by UV-visible spectroscopy) remains unchanged for millions of pulses thereafter. Such behavior indicates that the formation of color centers is facilitated by preexisting defects, be they intrinsic defects or impurities. Large variations in the amount of laser-induced color centers were observed between vendors, grades, and even from crystal-to-crystal. As with fused silica, it is apparent that the crystal growing process for fluorides for 193-nm applications has not yet been fully optimized.

3. Pellicles

Damage-resistant pellicles are being developed by several vendors for use at 248–250 nm. These free-standing membranes are typically ~ 1 μm thick and are highly transparent at their intended wavelength of use. They are made of organic materials with a large concentration of C–F bonds. Such bonds are both chemically and photochemically stable. We have evaluated several of the 248-nm pellicles for use at 193 nm,[2] and have found that they are transparent at 193 nm as well. They do degrade, and eventually rupture, upon exposure to 193-nm radiation, probably via a combination of one- and two-photon processes (Fig. 2). Nevertheless, the fluence scaling laws predict that such pellicles will change very little over many years of full-time operation. It thus appears that the 248-nm pellicle technology can be readily adapted to 193 nm.

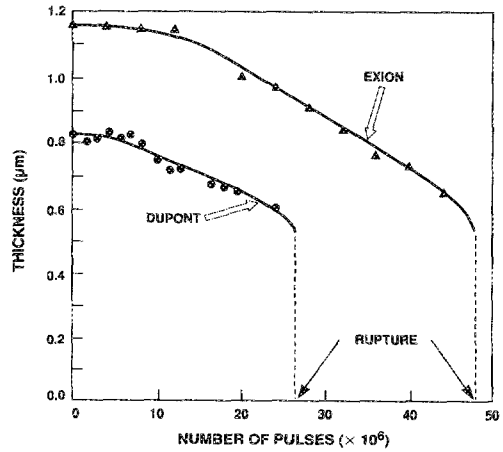

FIG. 2. Excimer induced thinning of pellicles from DuPont and Exion. The initial thicknesses were 0.83 and 1.17 μm, respectively. The laser was operated at 193 nm, at a fluence of 5 mJ cm^{-2}/pulse.

III. PHOTORESISTS

A. Single-layer resists

The primary issue for traditional, wet developed, ~ 1-μm-thick single-layer resists at 193 nm is high optical absorbance. Conventional novolac- or poly(vinylphenol)-based resins have absorption coefficients exceeding 10^5 cm^{-1} at 193 nm, which corresponds to a photon penetration depth of less than 100 nm. The primary reason for this strong absorbance is the π–π^* electronic transition which occurs in aryl-containing systems at wavelengths near 200 nm. Polymeric resins containing no aryl functionality, such as poly(methylmethacrylate) (PMMA) have much lower absorption coefficients, typically less than 10^4 cm^{-1}. This fact has led to the use of PMMA for characterizing prototype imaging optics at 193 nm.[3,4] However, PMMA has low sensitivity (roughly 1 J/cm^2 at 193 nm). More sensitive acid-catalyzed resist systems, also based on acrylate resins, have been proposed and are under development.[5,6] The drawback to using these acrylate-based resists is a reduced plasma-etch resistance, as compared to novolac resins. One approach to improve etch resistance is to produce resins with large, alicyclic pendant groups on the backbone, such as adamantyl methacrylate.[5] This approach improves etch resistance to near that of novolacs for some plasma chemistries. Postdevelopment incorporation of silicon, e.g., via silylation, is another general approach to improve etch resistance, although additional process steps would be required.

B. Surface imaging

An alternative to single-layer resists is the use of multilayers or surface imaging. These strategies were initially developed for use at longer wavelengths to reduce some of the problems due to small optical depths-of-focus and to the reflectivity associated with single-layer processing. These same approaches have proven to be enabling technologies for 193-nm lithography. Silylation processes, in particular, have seen increasing emphasis as an alternative to single-layer lithography at longer wavelengths and are well suited for 193-nm lithography. For the 193-nm process, silylation is generally a positive-tone process, as shown in Fig. 3, due to the laser-induced crosslinking.[7] This crosslinking hinders the diffusion of silicon into the exposed portions of the resist, which are subsequently developed in an anisotropic oxygen plasma treatment. It should be noted that this process is of the opposite tone to that of the DESIRE process used at longer wavelengths, which relies on thermal crosslinking to achieve silylation selectivity.[8]

While some resists have been specifically designed to crosslink upon exposure at longer wavelengths (e.g., SNR 248 at 248 nm), the high photon energy at 193 nm leads to efficient crosslinking of the novolac or polyvinylphenol res-

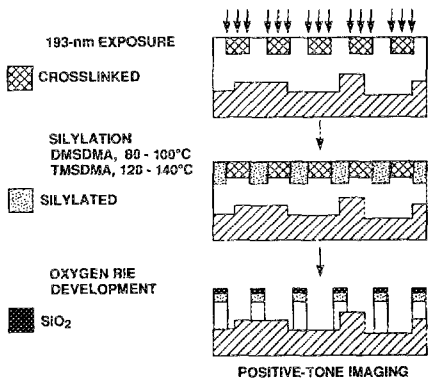

FIG. 3. Schematic of 193-nm positive-tone silylation process showing exposure, silylation, and etching steps.

ins that many resists are constituted from.[9] The highest sensitivities, however, are found for the chemically amplified resists. These range from 2 to 15 mJ/cm^2, depending on postexposure baking conditions. The sensitivity for some polyvinylphenol resins is not much lower, however, with a best value to date of 20 mJ/cm^2.

The process optimization for a silylated resist requires an understanding of the exposure, silylation, and etching steps, each of which has significant interactions with the other. While the laser-induced crosslinking accounts for the silylation selectivity, the silylation profile in the resist is a function of the silylation conditions and the specific resist and silylating reagent combination. The ultimate linewidths and process control are determined by the response of this silylated profile to the etching process. For a positive-tone process, the silylation profile is governed by the diffusion process of the reagent through the crosslinked latent image in the exposed resist film. This diffusion process is generally characterized as a "case II type," since the time scales for diffusion and polymer relaxation are comparable.[10] Two distinguishing features of case II diffusion (contrasted with Fickian diffusion) are a linear increase in diffusion depth with time (instead of a square-root-dependence) and a sharp interface between the silylated and unsilylated portions of the resist (instead of complementary error-function-type profile). Each of these features has been observed experimentally.[11]

The scanning electron micrographs (SEM) in Fig. 4 demonstrate a plasma staining technique[12] which enables the silylated profile to be observed. The series of micrographs show a variation in the depth of silylation as a function of feature dimension. This decrease, which can be as much as a 50% reduction in silylation depth between large and small features, is due in part to crosslinking which results from the degraded aerial image of smaller features near the diffraction limit of the stepper. A model was developed to account for the effect of aerial image, and it was found that only half of the decrease could be attributed to it. The particular diffusion characteristics of the silylation process explain the additional effect, since the silylation rate for a case II process is related to the stress induced by the swelling during silylation.[10] At smaller features, the proximity of the exposed parts of the film restricts the amount of swelling which can occur and limits the total amount of silylation. This same effect explains the variation in silylation depth for isolated lines and grating structures of the same dimension, since the amount of crosslinking in the exposed area next to an isolated line is greater than for a line-and-space grating. Efforts to improve this model and incorporate the swelling effects are continuing.

The overall contrast of the silylation process is quite high (on the order of 20 or more), based primarily on the

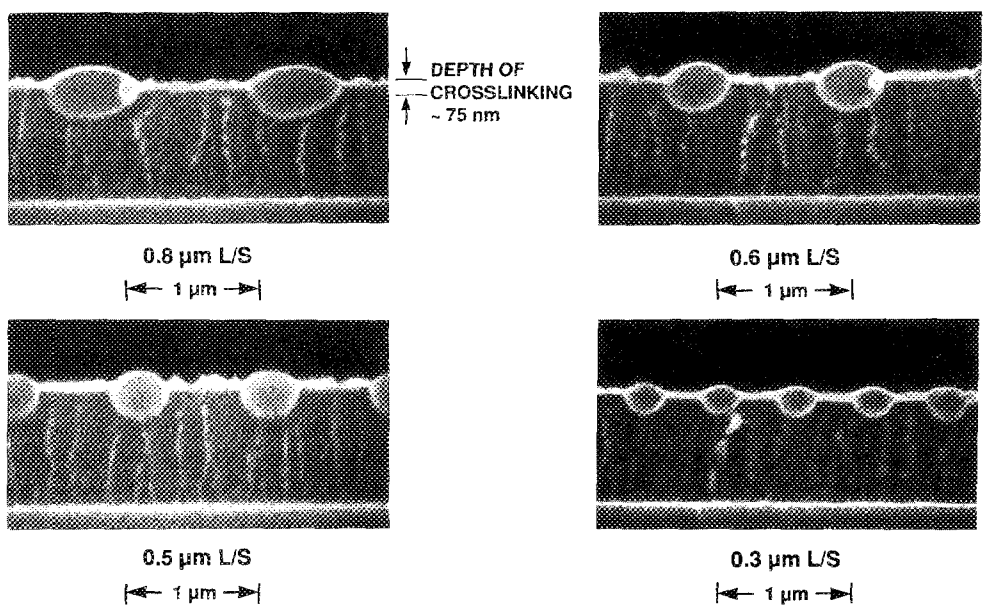

FIG. 4. Scanning electron micrographs (SEMs) of the silylation profiles in polyvinylphenol resist silylated at 100 °C for 3 min with 10 Torr of DMSDMA. Equal line-and-space grating structures with feature sizes of 0.8, 0.6, 0.5, and 0.3 μm are shown.

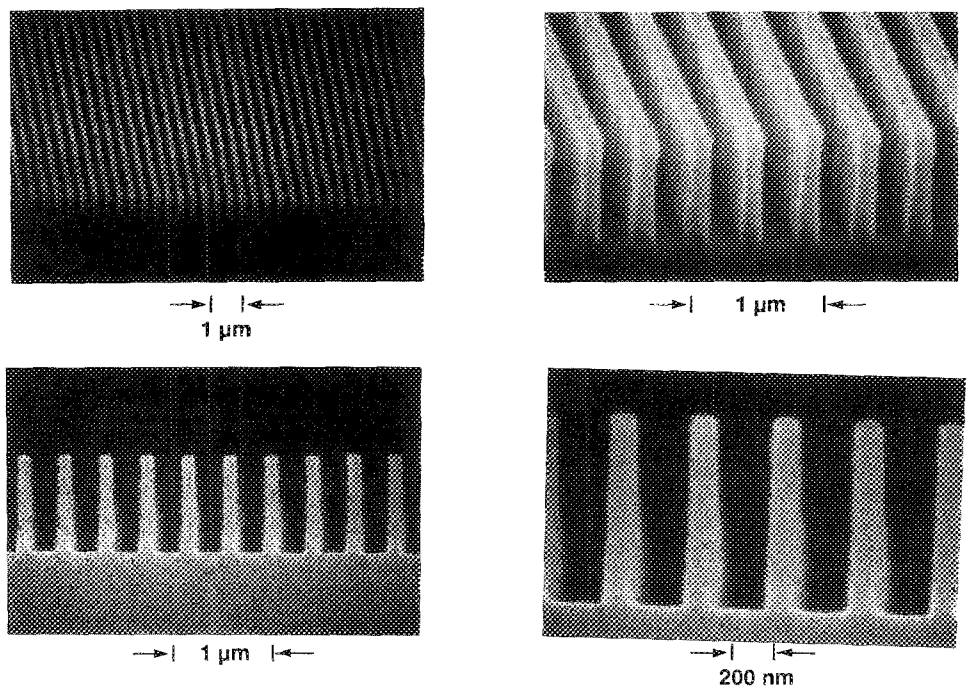

FIG. 5. Resolution of 0.2-μm line-and-space gratings in polyvinylphenol resist silylated at 140 °C for 1 min with trimethylsilyldimethylamine. The pattern was exposed to 60 mJ/cm^2 and developed in an oxygen plasma at 20 mTorr and -250 V bias.

nonlinearity in oxygen etching with silicon incorporation. Measurements based on Fourier-transform infrared (FTIR) spectroscopy show a much lower contrast (1.3) for the silicon incorporation. Under typical processing conditions, only 30 nm of silylated resist are required to withstand the etching of a 1-μm-thick unsilylated film. Etch selectivities between silylated and unsilylated resist range from 16:1 to 50:1, depending on the plasma reactor-type and processing conditions.

Two important criteria during the plasma etching step are anisotropic etching and the absence of residue after processing. Most plasma etching tools are capable of producing near-vertical sidewalls, given an appropriate substrate bias. The substrate bias also plays an important role in the generation of residue, however, since too large a bias can cause sputtering of the protective silicon oxide mask which is formed in the silylated areas. We have found that parallel-plate, reactive ion etching (RIE) plasmas with bias voltages above 150 V typically result in residue, while high-ion-density plasmas with biases between 30 and 100 V usually do not show residue.

The resolution and process latitude were evaluated using a 193-nm stepper with a 5× reduction catadioptric lens having an effective NA of 0.22.[13] For 0.4-μm line-and-space gratings (equivalent to a k_1 factor of 0.46) the depth-of-focus was found to be $\sim$4 μm, in agreement with the Rayleigh estimate. The exposure latitude, defined by the range of doses which print the features within 10% of the nominal linewidth, was determined to be 12% for the 0.4-μm line-and-space gratings. The highest resolution imaging with silylation possible from this stepper (NA=0.33) is shown in Fig. 5, which depicts 0.2-μm line-and-space grating structures printed in polyvinylphenol resist.

C. Bilayer resists

In parallel with the development of the positive-tone silylation process described above we have also developed negative-tone bilayer processes optimized for 193-nm lithography. These bilayers consists of a thin (20–100 nm) silicon-containing imaging layer spun on a thicker ($\sim$1 μm) organic planarizing layer. Both two-dimensional (polysilanes) and three-dimensional (3D) (polysilynes) silicon-backbone networks have been studied. In all these instances the principal electronic transition when irradiated at 193 nm is the σ–σ^* transition resulting from σ conjugation of the all-silicon backbone. Following this excitation, reaction pathways leading to scission of the Si–Si bonds result in efficient photodegradation of the Si backbone. In the presence of oxygen, this degradation results in siloxane (Si–O–Si) formation within the polymer, and in the case of 3D network polymers in a concomitant increase in molecular weight. The efficiency of photoinduced polymer degradation can be further enhanced by addition of sensitizers. Silicon polymers containing pendant aryl groups exhibit the greatest sensitivity enhancement, probably due to favorable pathways for electron transfer between the pendant aryl groups and the sensitizer. These photosensitization processes have been studied in detail for the poly(phenylalkylsilanes), where detailed mechanisms for the sensitivity enhancement have been proposed.[14]

Following photooxidation of the imaging layer, pattern-

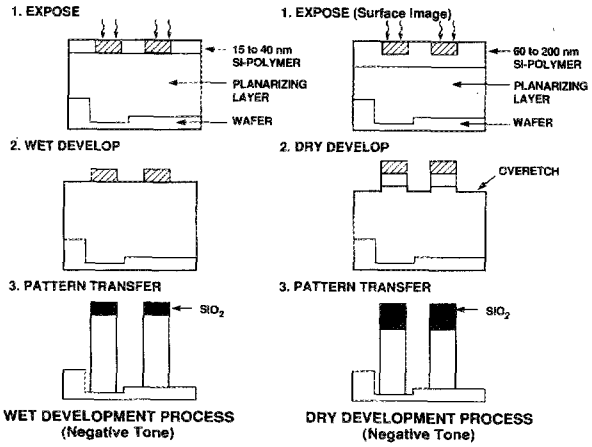

FIG. 6. Schematic diagram of process flow for bilayer lithography. The left-hand part shows the process flow for a wet-developed imaging layer, whereas the right-hand part is for a plasma-developed bilayer. In either case, the pattern transfer is performed using oxygen RIE.

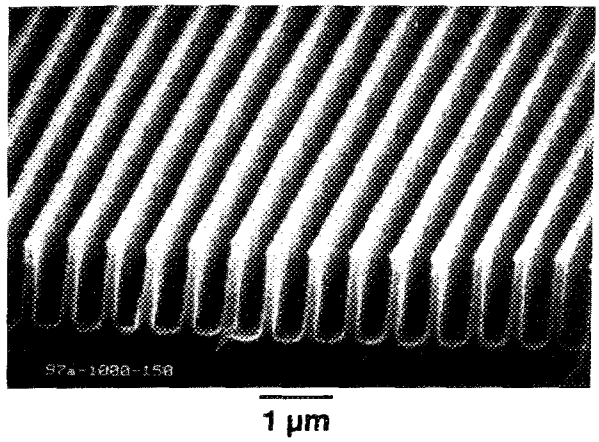

FIG. 7. SEM of 0.2-μm lines-and-spaces printed in 30-nm-thick poly(*n*-butylsilyne) on 1-μm-thick hard-baked SI813 using an exposure dose of 50 mJ/cm^2. The pattern transfer was with oxygen RIE.

ing is completed either by wet or dry development, followed by pattern transfer into the planarizing layer, as described below.

1. Wet development

As mentioned above, exposure of network silicon polymers, such as the polysilynes, to 193-nm radiation results in molecular weight increases due to oxidative crosslinking. This crosslinking renders the polymer insoluble, resulting in negative-tone imaging. For successful wet development, however, the crosslinked latent image must extend through the entire resist film thickness. This limits film thicknesses that can be used for wet development to under 50 nm (see Fig. 6), due to the high optical absorbance at 193 nm. This limitation places demands on the oxygen-plasma pattern transfer step, as discussed below.

The optimal formulations for wet development are typically copolymers of monomers which would normally give high- and low-molecular weight homopolymers.[15] This combination allows control of both molecular weight and solubility parameter, which in turn determine the resist sensitivity. In general, these systems require 35–85 mJ/cm^2 at 193 nm to become insoluble. The contrast of 30-nm-thick films is typically between 5 and 10. When coupled with the high nonlinearity of the oxygen-plasma-based pattern transfer, the overall process contrast is greater than 20.

Additional improvements in sensitivity can be obtained by either of two methods. First, electrophilic sensitizing agents, such as 2,4,6,-trichloromethyl-1,3,5,-triazine, can be added. These agents act similarly to those proposed for positive-tone silicon-polymer resists.[14] As described earlier, the enhancement in sensitivity depends on the number of pendant aryl groups, with a twofold improvement in sensitivity observed for 100% aliphatic-substituted systems and sixfold improvement for 100% aromatic systems. An alternative method for improving the photosensitivity of polysilynes involves the preparation of the polysilyne with an electron-withdrawing group pendant directly to the backbone. Sensitivities of 1–10 mJ/cm^2 have been obtained with this approach.

Figure 7 shows an example of 0.2-μm lines printed in poly(*n*-butylsilyne). The pattern transfer into the planarizing layer was performed using RIE. In addition, Al/Si electrical test structures have successfully been fabricated using BCl_3 plasma chemistry for the Al/Si etch. The bilayer resist system can either be wet stripped using commercially available solutions or dry stripped using a CF_4 plasma.

2. Dry development

The efficient photooxidation mentioned earlier also results in a reduced etch rate relative to the unexposed polymer in bromine-based plasmas, thus enabling dry (plasma) development. Evaluation of the development step using various etching tools has indicated the importance of the plasma conditions for optimization of both the resist sensitivity and contrast. In particular, the independent control of the ion and neutral fluxes at the wafer surface is important for process optimization.[16] A large radical-induced chemical component to the resist development is necessary relative to contributions from physical sputtering. Typically, the development is performed at low wafer bias (<100 V) and high-plasma power. The etch rate selectivity of unexposed to exposed polymer is typically between 2:1 and 5:1, whereas the contrast (nonlinearity) for the etch step has been measured from 0.2 to 5, depending on the development conditions. These contrast values are lower than those obtained for wet development, and this fact reduces the lithographic process windows. For example, at $k_1=0.57$ (0.5-μm feature, 193 nm, 0.22 NA) we have measured an exposure latitude of $\sim$10%, as compared to 35% for wet development. These values were obtained using the same oxygen reactive ion etcher under identical conditions.

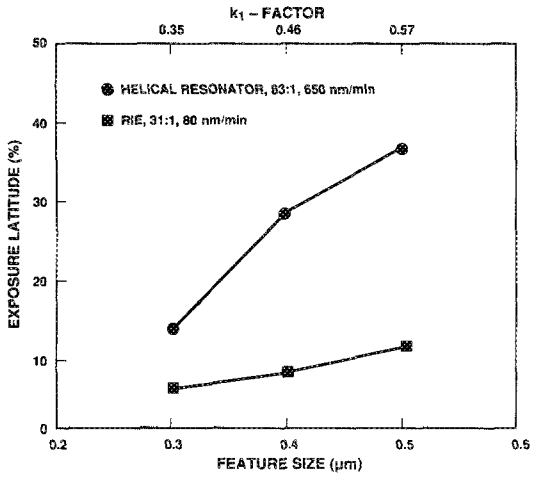

FIG. 8. Exposure latitude vs feature size for a poly(*n*-propylsilyne)-co-poly(*i*-butylsilyne) resist. The two curves represent differences that result from use of a parallel plate vs helical resonator plasma source for the oxygen-plasma pattern transfer step. The etch selectivities and the etch rates of the planarizing layer are also indicated.

3. Pattern transfer

The use of thin imaging layers places strict demands on the pattern transfer step. Specifically, good control of both the critical dimensions (CD) and the sidewall slope is more difficult when using a thin imaging layer. In particular, line-edge erosion caused by ion bombardment from the plasma must be kept to a minimum during the etching of the planarizer layer. The absolute and relative etch rates of the silicon polymer and the planarizer are therefore important in determining the overall utility of these systems as photoresists. These values are in turn affected by the etching tool and the etching conditions. Figure 8 demonstrates the dramatic effect etch tool choice can play in CD control, where a threefold increase in exposure latitude is realized when using a helicon source over a parallel plate source. On certain high-ion-density etchers[17] etch selectivities between the planarizing layer (hard-baked AZ 1813) and polysilyne of 149:1 at planarizer etch rates approaching 1 μm/min have been achieved. Near-vertical profiles have been obtained under these conditions. A complete summary of the etch tool comparison is presented in Ref. 18.

IV. CONCLUSIONS

In this article we have reviewed the current status of the Lincoln Laboratory efforts on 193-nm photolithography. The construction of a 0.5-NA projection system capable of 0.25-μm resolution with no phase-shifting masks over large fields (22 by 35 mm) is nearing completion. This step-and-scan system is similar conceptually and in many practical aspects to commercially available production-oriented systems for use at ~250 nm, which are designed for ~0.35-μm resolution. The shift from 250 to 193 nm changes quantitatively, if not qualitatively, the effects of laser irradiation on the optical materials used in these projection systems. Extensive studies of fused silica and several crystalline fluorides indicate that highly transparent materials at 193 nm are available, and that a properly constructed stepper will perform within specifications for a decade or more of full-time operation.

The change in wavelength also implies that new resist strategies, specially optimized for 193-nm application, need to be developed. Initial results show that conventional single-layer resist technologies can be extended to this new wavelength, although they may utilize new resin formulations. Our main resist-development effort has concentrated on two other approaches: surface imaging (silylation) and bilayer resists. Using both methods we have demonstrated better than 0.2-μm resolution, and have engineered the processes to achieve high photosensitivity, wide latitudes, and absence of etch residue.

Further qualification of the resist performances is still required, and of course the performance of the step-and-scan system awaits careful evaluation. Nevertheless, our results to date indicate that 0.25-μm, 193-nm lithography is indeed a viable and robust technology. Furthermore, it is extendible (with phase-shifting masks, higher NAs, and new illumination methods) to 0.18-μm, and possibly smaller dimensions.

ACKNOWLEDGMENTS

The authors thank C. A. Bukowski, S. Cann, J. E. Curtin, D. M. Craig, C. L. Dennis, W. F. DiNatale, D. K. Downs, L. M. Eriksen, C. Marchi, B. Maxwell, and R. W. Otten for their expert technical assistance. The authors also thank the members of our technical advisory board for their comments, advice, and insight. This work was sponsored by the Defense Advanced Research Projects Agency.

[1]M. Rothschild, D. J. Ehrlich, and D. C. Shaver, Appl. Phys. Lett. **55**, 1276 (1989).
[2]M. Rothschild and J. H. C. Sedlacek, Proc. SPIE **1674**, 618 (1992).
[3]M. Sasago, Y. Tani, M. Endo, and N. Nomura, Proc. SPIE **1264**, 466 (1990).
[4]Y. Ozaki, Y. Kawai, and A. Yoshikawa, Jpn. J. Appl. Phys. **29**, 2553 (1990).
[5]Y. Kaimoto, K. Nozaki, S. Takechi, and N. Abe, Proc. SPIE **1672**, 66 (1992).
[6]R. D. Allen, G. M. Wallraff, W. D. Hinsberg, and L. L. Simpson, Proc. Am. Chem. Soc. **66**, 251 (1992).
[7]M. A. Hartney, R. R. Kunz, D. J. Ehrlich, and D. C. Shaver, Proc. SPIE **1262**, 119 (1990).
[8]J. P. W. Schellekens and R. J. Visser, Proc. SPIE **1086**, 220 (1989).
[9]M. A. Hartney, D. W. Johnson, and A. C. Spencer, Proc. SPIE **1466**, 238 (1991).
[10]N. L. Thomas and A. H. Windle, Polymer **529**, 23 (1982).
[11]M. A. Hartney, M. Rothschild, R. R. Kunz, D. J. Ehrlich, and D. C. Shaver, J. Vac. Sci. Technol. B **8**, 1476 (1990).
[12]C. M. Garza, G. Misium, R. R. Doering, B. Roland, and R. Lombaerts, Proc. SPIE **1086**, 229 (1989).
[13]D. C. Shaver, D. M. Craig, C. A. Marchi, M. A. Hartney, and F. Goodall, Proc. SPIE **1674**, 766 (1992).

[14]G. M. Wallraff, R. D. Miller, N. Clecak, and M. Baier, Proc. SPIE **1466**, 211 (1991).
[15]R. R. Kunz, M. W. Horn, P. A. Bianconi, D. A. Smith, and J. R. Eshelman, J. Vac. Sci. Technol. B **10**, 2554 (1992).
[16]R. R. Kunz, M. W. Horn, R. B. Goodman, G. M. Wallraff, R. D. Miller, E. J. Ginsberg, P. A. Bianconi, D. A. Smith, and J. R. Eshelman, Proc. SPIE **1672**, 385 (1992).
[17]Semicond. Inter. July, 52 (1992).
[18]M. W. Horn, M. A. Hartney, and R. R. Kunz, Proc. SPIE **1672**, 448 (1992).